PCCP

Accepted Manuscript

This is an *Accepted Manuscript*, which has been through the Royal Society of Chemistry peer review process and has been accepted for publication.

Accepted Manuscripts are published online shortly after acceptance, before technical editing, formatting and proof reading. Using this free service, authors can make their results available to the community, in citable form, before we publish the edited article. We will replace this *Accepted Manuscript* with the edited and formatted *Advance Article* as soon as it is available.

You can find more information about *Accepted Manuscripts* in the Information for Authors.

ROYAL SOCIETY OF CHEMISTRY

www.rsc.org/pccp

Theoretical Study of the Coordination Behavior of Formate and Formamidoximate

with Dioxovanadium (V) Cation: Implications for Selectivity towards Uranyl

Nada Mehio[1], J. Casey Johnson,[2] Sheng Dai[1, 2], Vyacheslav S. Bryantsev[2*]

[1]*Department of Chemistry, University of Tennessee, Knoxville TN 37996 US*

[2]*Chemical Sciences Division, Oak Ridge National Laboratory, Oak Ridge TN 37831 US*

Email: bryantsevv@ornl.gov

Phone: (865) 576-4272

Fax: (865) 576 7956

1

Abstract

Poly(acrylamidoxime)-based fibers bearing random mixtures of carboxylate and amidoxime groups are the most widely utilized materials for extracting uranium from seawater. However, the competition between uranyl (UO_2^{2+}) and vanadium ions poses a significant challenge to the industrial mining of uranium from seawater using the current generation of adsorbents. To design more selective adsorbents, a detailed understanding of how major competing ions interact with carboxylate and amidoxime ligands is required. In this work, we employ density functional theory (DFT) and wave-function methods to investigate potential binding motifs of the dioxovanadium ion, VO_2^+, with water, formate, and formamidoximate ligands. Employing higher level of theory calculations (CCSD(T)) resolve the existing controversy between the experimental results and previous DFT calculations for the structure of the hydrated VO_2^+ ion. Consistent with the EXAFS data, CCSD(T) calculations predict higher stability of the distorted octahedral geometry of $VO_2^+(H_2O)_4$ compared to the five-coordinate complex with a single water molecule in the second hydration shell, while all seven tested DFT methods yield the reverse stability of the two conformations. Analysis of the relative stabilities of formate-VO_2^+ complexes indicates that both monodentate and bidentate forms may coexist in thermodynamic equilibrium in solution. Investigations of VO_2^+ coordination with the formamidoximate anion has revealed the existence of seven possible binding motifs, four of which are within ~ 4.0 kcal/mol of each other. Calculations establish that the most stable binding motif entails the coordination of oxime oxygen and amide nitrogen atoms via a tautomeric rearrangement of amidoxime to imino hydroxylamine. The difference in the most stable VO_2^+ and UO_2^{2+} binding conformation has important implications for the design of more selective UO_2^{2+} ligands.

1. Introduction

Due to the high carbon emissions associated with the diminishing global supply of fossil fuels, there has been great interest in developing alternative sources of energy. In light of this interest, extensive research efforts spanning multiple decades have focused on developing a commercial method for mining uranium from seawater.[1] While there is an estimated 4.5 billion tons of uranium dissolved in seawater, largely in the form of uranyl tricarbonate,[2-4] $UO_2(CO_3)_3{}^{4-}$, there are a number of challenges associated with developing an adsorbent material capable of extracting uranium from seawater. These challenges primarily stem from the fact that $UO_2{}^{2+}$ is present in very low concentrations, roughly 3 ppb,[2] while numerous competing metal cations are at much higher concentrations.[4] Currently, poly(acrylamidoxime) fibers are the most widely utilized adsorbents for mining uranium from seawater. Poly(acrylamidoximes) were first identified in a screening of 200 organic polymers as the only adsorbent capable of extracting $UO_2{}^{2+}$ from pH 8.3 aqueous solutions, the approximate pH of seawater.[5, 6] However, poly(acrylamidoxime) fibers are not perfectly selective towards $UO_2{}^{2+}$ in seawater. In particular, one of the greatest challenges associated with the commercial use of poly(acrylamidxoime) fibers is the competition between $UO_2{}^{2+}$ and vanadium ions.[7] In addition to reducing the $UO_2{}^{2+}$ capacity of poly(acrylamidoxime) fibers, vanadium cations bind so strongly that striping the cations irreversibly damages the adsorbent.[1, 8] Due to the near order of magnitude difference in concentrations in seawater, this paper we will focus on vanadium(V) species rather than vanadium(IV).[7, 9] More specifically, the orthovanadate ion, $H_2VO_4{}^-$, is in equilibrium with the pervanadyl ion, $VO_2{}^+$, in aqueous solutions:

$$H_2VO_4^- + 2H^+ \leftrightarrows H_3VO_4 + H^+ \leftrightarrows VO_2^+ + 2H_2O \qquad \textbf{(Eq. 1)}$$
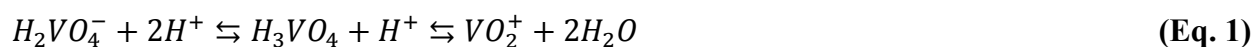
However, in slightly basic conditions, such as seawater, the orthovanadate is the dominant species. Nevertheless, the equilibrium can be shifted to the right in the presence of organic ligands capable of interacting with the VO_2^+ cation.[7-9] For example, Rogers et al.[10] demonstrated that an amidoximate-VO_2^+ complex can be crystallized from neutral solutions. Thus, understanding how poly(acrylamidoxime) fibers interact with the VO_2^+ cation is essential for the rational design of subsequent generations of chelating polymer adsorbents.
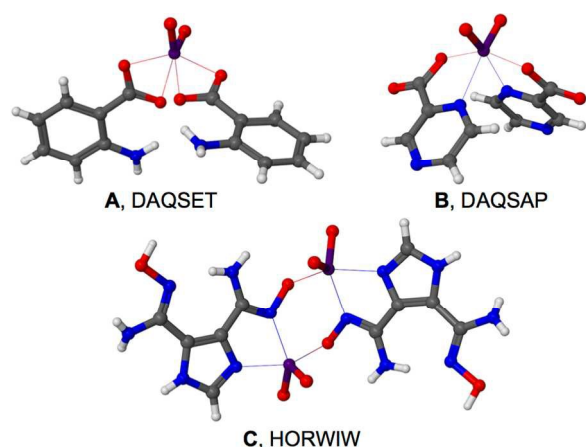
Figure 1. Crystal structures of amidoximate-VO_2^+ and carboxylate-VO_2^+ complexes. The DAQSET complex and the DAQSAP complex are representative of the two carboxylate-VO_2^+ binding modes observed in the CSD. The HORWIW complex is the only reported amidoximate-VO_2^+ crystal structure.

Current state-of-the-art adsorbents based on poly(acrylamidoxime) fibers are based on a random copolymer of carboxylate and amidoxime monomers at a 40:60 monomer ratio, respectively.[11, 12]   Therefore, in order for the interactions between poly(acrylamidxoimes) and VO_2^+ cations to be understood, the binding motif of simple, representative carboxylate and amidoxime ligands with VO_2^+ needs to be established. While a wide variety of carboxylate-VO_2^+ crystal structures can be found in the Cambridge Structural Database (CSD),[13] only two crystal structures with pure carboxylate binding motifs can be found. One of these crystal structures, DAQSET,[14] is illustrated in **Figure 1A**. The majority of the carboxylate-VO_2^+ crystal structures exhibit a mixed binding motif consisting of a monodentate-carboxylate and an amine nitrogen, a pyridine nitrogen, or an ether oxygen chelate. An example of one of these mixed chelate

structures, DAQSAP,[14] is illustrated in **Figure 1B**. Moreover, the coordination number of the carboxylate-monoVO$_2^+$ crystal structures reported on the CSD varied between five and six. A coordination number five was observed if the carboxylate ligand was rigid, sterically strained, or contained electron withdrawing groups. Furthermore, although Rogers et al.[10] demonstrated the formation of a dimeric complex of a 4,5-di(amidoxime)-functionalized imidazole ligand with the VO$_2^+$ ion (HORWIW, **Figure 1C**), the binding motifs with pure amidoxime ligands to VO$_2^+$ have yet to be established.

In addition to the various ligand-VO$_2^+$ binding motifs, there is also a disagreement between the experimental and density functional theory (DFT) calculations for the structure of the hydrated VO$_2^+$ ion. Extended X-ray absorption fine structure (EXAFS) and large-angle X-ray scattering (LAXS) data show that the hydrated VO$_2^+$ ion adopts a very distorted octahedral configuration.[15] In contrast, static B3LYP calculations suggested that the first shell hydration structure for VO$_2^+$ consisted of only three water molecules.[16] Furthermore, Car-Parinello molecular dynamics (MD) simulations performed using the BP86 density functional predicted the hydrated VO$_2^+$ structure to be approximately an equal mixture of the five- and six-coordinate structures.[17] The application of higher levels of theory is crucial to resolve the inconsistency of experimental and theoretical results.

Herein, we report the results of a computational investigation of the interactions of the dioxovanadium (V) ion, VO$_2^+$ with formate and formamidoximate anions. The chosen ligands are small enough that high-level *ab initio* calculations are readily performed. To resolve the discrepancy between the experimental[15] and computed[16, 17] structures of hydrated VO$_2^+$ complexes, we used as benchmarks calculated relative energies obtained at the coupled-cluster theory with single, double, and perturbative triple excitations (CCSD(T)) in the aug-cc-pVDZ

basis set. Calculations at various levels of theory, such as CCSD(T)/aug-cc-pVDZ, MP2/aug-cc-pVQZ, and several DFT/aug-cc-pVDZ methods including Grimme's DFT-D3 dispersion correction were applied to identify how carboxylate and amidoximate ligands interact with the VO_2^+ ion. This understanding provides an important step for developing a computational protocol for predicting the log K values for the formation of VO_2^+ complexes and lays the foundation for the rational design of ligands that are more selective for the UO_2^{2+} ion.

2. Methods

Electronic structure calculations were carried out using the Gaussian 09 Revision D.01[18] and NWChem 6.5 software packages.[19] CCSD(T) calculations[20-22] were employed with the aug-cc-pVDZ basis set[23, 24] to determine the benchmark relative energies of VO_2^+ complexes, in which Moller-Plesset perturbation theory (MP2) method[25, 26] and density functionals[27, 28] are evaluated against. Geometry optimizations were performed at the MP2 and DFT levels using the aug-cc-pVDZ basis set, except for the bare VO_2^+ cation, where the highest level of theory used was CCSD(T)/aug-cc-pVTZ. Only the valence electrons on C, N, and O and the subvalence electrons (3s, 3p) on V were correlated in the MP2 and CCSD(T) calculations.

We used a family of augmented correlation-consistent basis sets[23, 24] (aug-cc-pVnZ, n = D, T, Q) for the basis set expansion in the MP2 calculations. The CCSD(T) binding energies at the aug-cc-pVQZ level of theory were estimated with the following equations:

$$CCSD(T) + \delta MP2 = \Delta E(CCSD(T)/aug\text{-}cc\text{-}pVDZ//MP2/aug\text{-}cc\text{-}pVDZ) + \delta MP2 \qquad \textbf{(Eq. 2)}$$

$$\delta MP2 = \Delta E(MP2/aug\text{-}cc\text{-}pVQZ//MP2/aug\text{-}cc\text{-}pVDZ) - \Delta E(MP2/aug\text{-}cc\text{-}pVDZ) \qquad \textbf{(Eq. 3)}$$

Zero-point energies (ZPE) and thermal corrections were obtained at the MP2 level without scaling using the effective core potential (ECP)[29-32] LANL2TZ basis set for vanadium and the 6-311++G(d,p) basis set for the other atoms.

While there is a general consensus that DFT is better suited than MP2 for the study of open-shelled systems involving metal ion center,[33] the performance of MP2 for closed-shell systems involving a metal ion center remains unclear. In order to determine the optimal level of theory for studying these systems, we examined the ability of seven density functionals to reproduce the benchmark electronic binding energies (CCSD(T) + δMP2) of VO_2^+ complexes. The density functionals tested include one Generalized Gradient Approximation (GGA) functional (PBE[34, 35]), three hybrid GGA functionals (B3LYP,[36, 37] ωB97xD,[38, 39] and B97D3[40, 41]), two local meta-GGA functional (M06-L[42] and TPSS[43]), and one hybrid meta-GGA functional (M06[42]). The aug-cc-pVDZ basis set was employed in all DFT calculations. We found that DFT and MP2 methods could give different geometries of VO_2^+ complexes, where in some cases the six-coordinate complexes were stationary point only at the MP2 level and four-coordinate complexes were stationary points only at the DFT level. In light of this discrepancy, Grimme's D3 dispersion corrections[44] were applied to B3LYP, PBE, TPSS, and M06-L density functionals to provide a better account of noncovalent interactions. Single-point CCSD(T)/aug-cc-pVDZ calculations using MP2/aug-cc-pVDZ and B3LYP/aug-cc-pVDZ geometries were performed to determine the sensitivity of the CCSD(T) relative energies to changes in geometries of VO_2^+ complexes obtained at different levels of theory.

A transition state search with the B3LYP/aug-cc-pVDZ method was performed using a standard Berny algorithm implemented in Gaussian,[18] starting from the partially optimized

7

geometry at the same level of theory along the chosen reaction coordinate and the precalculated Hessian. Intrinsic reaction coordinate calculations (IRC) were performed to ensure that transition-state structures connect their respective reactants and products.

Using the gas phase geometries obtained at the MP2/aug-ccpVDZ level, implicit solvent corrections were obtained with the IEF-PCM model[45-47] in Gaussian 09, using the default atomic radii of the universal force field (UFF). Electronic energies in the solvent reaction field were computed using the ECP LANL2TZ basis set for vanadium and the 6-31+G(d) basis set for the other atoms. Relative energies in aqueous solutions were reported by combining electronic energies at the CCSD(T)/aug-cc-pVDZ + δMP2 level of theory, with ZPE and thermal corrections obtained at the MP2/LANL2TZ(V)/6-311++G(d,p) level and the solvation energies calculated using the IEF-PCM solvation model.

3. Results and Discussion

As noted in the Introduction, there is an incompleteness of data describing the binding modes and coordination numbers of amidoximate-VO_2^+ and pure carboxylate-VO_2^+ complexes. In order to supplement this lack of data, we computationally elucidated binding modes and coordination numbers of formamidoximate-VO_2^+ and formate-VO_2^+ complexes. First, we analyzed the bonding nature in the VO_2^+ cation, which provides the foundations for understanding the coordination properties of this oxoion, in addition to highlighting the potential limitations of the MP2 and DFT methods in predicting the structure of VO_2^+ complexes. Second, we resolved the discrepancy between the experimental results and previous DFT calculations for the structure of the hydrated VO_2^+ cation. Next, we determined the optimal coordination numbers and binding modes of formate-VO_2^+ and formamdioxime-VO_2^+ complexes. Finally, corroborated

by crystal structure analysis, the theoretical results suggest a strategy for the design of amidoxime ligands that are more selective toward the uranyl ion.

3.1 VO$_2^+$ Cation in the Gas Phase

To lay the groundwork for a clear understanding of the potential ligand binding motifs, it is necessary to first understand the structure and electronic properties of the bare VO$_2^+$ cation. Due to the absence of an experimental VO$_2^+$ gas phase geometry, the structural properties, i.e. bond distances and angles, are obtained from the CCSD(T) optimized structure and used as benchmarks against the DFT and MP2 predicted structure. As seen in Table 1, the MP2 optimized structures overestimate the V=O bond distance while underestimating the O=V=O bond angle, whereas the DFT optimized structures underestimate the V=O bond distance and overestimate the O=V=O bond angle. Consequentially, MP2 leads to an overestimation of the coordination number for VO$_2^+$, while DFT leads to an underestimation of the coordination number for VO$_2^+$.

Figure 2 shows the five highest occupied molecular orbitals (HOMOs) obtained at the B3LYP/aug-cc-pVDZ level of theory, illustrating the vanadium and oxygen bonding nature. HOMO-5 represents a σ bond between oxygen p_y and vanadium $d_{x^2-y^2}$ atomic orbitals (AOs). An additional σ bond is seen in HOMO-4, formed from the oxygen p_x and the vanadium d_{xy} AOs. HOMO-3 and HOMO-2 represent π bonds between oxygen p_z and vanadium d_{xz} and d_{xz} AOs, respectively. HOMO-1 represents a weakly bonding interaction between oxygen p_x vanadium d_{z^2} AOs and, finally, the HOMO represents non-bonding oxygen p_y AOs.

Table 1. Geometrical parameters of VO_2^+ in the gas phase.[a]

Theory	V=O (Å)	O=V=O (Degrees)
MP2	1.609	101.68
MP2/aug-cc-pVTZ	1.620	101.20
CCSD(T)	1.572	105.19
CCSD(T)/aug-cc-pVTZ	1.570	105.43
B3LYP	1.550	105.91
M06	1.540	105.91
M06-L	1.559	106.22
ωB97XD	1.535	106.03
B97D3	1.560	105.61
PBE-D3	1.565	105.51
TPSS-D3	1.567	105.56
M06-L-D3	1.559	106.22
B3LYP-D3	1.559	106.22

[a]The aug-cc-pVDZ basis set was employed in all calculations unless otherwise specified.
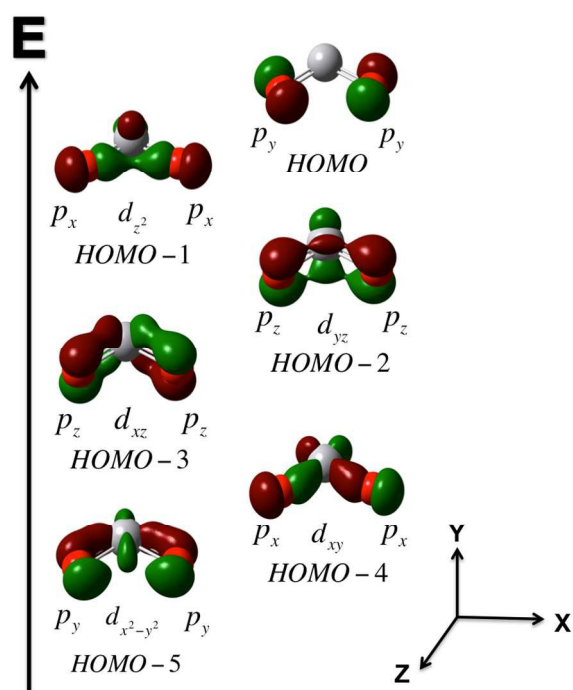
Figure 2. Several occupied molecular orbitals (MOs) illustrating the bonding in the VO_2^+ cation. Dominant atomic contributions to each MO are shown. The MOs were obtained at the B3LYP/aug-cc-pVDZ level of theory with an MO isovalue surface of 0.04 $(e/Å^3)^{1/2}$.

We note that the weakly bonding HOMO-1 orbital becomes a non-bonding orbital in the octahedral complex with four water molecules. In contrast to linear UO_2^{2+} that forms two σ-bonds with $5f_z^3$ and $6d_z^2$ AOs at the angle of 180°,[48] the availability of only d-orbitals in transition metals results in the geometry of dioxometal ions that is always bent. Moreover,

comparison of the U≡O bond in UO_2^{2+} and the V=O bond in VO_2^+ reveals that the oxygen atoms in VO_2^+ are more capable of engaging in hydrogen bonded interaction than those in UO_2^{2+}; the latter only very weakly interacts with hydrogen bond donors.[48] The extent to which the d-orbitals on vanadium are available for interaction with ligand orbitals depends on the strength of interaction with the vanadyl oxygen atoms. For example, *d*-orbitals involved in the formation of σ-bonds between vanadium and oxygen will be the least available for bonding with ligands. Consequentially, for VO_2^+ in a distorted octahedral geometry, ligands occupying equatorial positions on opposite sides of the V=O bond are always more weakly bound (having longer bonds) than ligands occupying axial positions perpendicular to the VO_2^+ plane.

3.2 Hydrolyzed VO_2^+ Complexes

As stated in the Introduction, the pervanadyl ion is not the dominant dioxovanadium (V) species in alkaline aqueous solutions, but rather in equilibrium (**Eq. 1**) with vanadic acid H_3VO_4 and the dominant orthovanadate $H_2VO_4^-$ species.[7-9] However, it has been demonstrated that this equilibrium can be shifted towards the VO_2^+ species in the presence of coordinating ligands.[10] In order to gain a better understanding of the aqueous chemistry of dioxovanadium (V), the relative energies of hydrated and hydrolyzed $VO_2(H_2O)_3^+$ complexes in the presence and absence of the formamidoximate ligand are compared. The MP2 optimized $VO_2(H_2O)_3^+$ complexes and their relative CCSD(T) + δMP2 Gibbs free energies in the gas phase and in aqueous solution can be found in **Figure 3**. The CCSD(T) + δMP2 results are consistent with experimental data, indicating that the hydrolyzed species, $H_2VO_3(H_2O)_2^+$ and $H_2VO_4(H_2O)^+$, are more stable than the hydrated cation, $VO_2(H_2O)_3^+$, in neutral aqueous solutions.

VO$_2$(H$_2$O)$_3$$^+$,
12.31 (12.01)

H$_2$VO$_3$(H$_2$O)$_2$$^+$,
0.00 (0.00)

H$_4$VO$_4$(H$_2$O)$^+$,
9.66 (3.38)
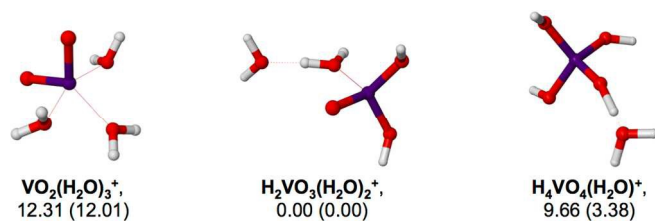
Figure 3. Structures of hydrated and hydrolyzed VO$_2$(H$_2$O)$_3$$^+$ complexes and relative energies in the gas phase and in aqueous solution (in parentheses) in units of kcal/mol.

While the hydrolyzed dioxovanadium(V) species are more stable than the hydrated VO$_2$$^+$ cation in neutral aqueous solution, in the presences of a binding ligand the equilibrium can be can be shifted towards VO$_2$$^+$.[10]   To explore this potential equilibrium change, the interaction between formamidoximate and dioxovanadium(V) in aqueous solution were computationally investigated with hydrated and hydrolyzed formamidoximate-dioxovanadum(V) complexes. While the results are sensitive to the number of water molecules in the complex, below we will only discuss the results for the largest complex studied, which contains three water molecules. Accordingly, the MP2 optimized VO$_2$(AO)(H$_2$O)$_3$ complexes and their relative CCSD(T) + δMP2 Gibbs free energies in the gas phase and aqueous solution can be found in **Figure 4**. As anticipated, the results obtained from CCSD(T) + δMP2 calculations indicate that the hydrated VO$_2$(AO)(H$_2$O)$_3$$^+$ complex is more stable than the hydrolyzed H$_2$VO$_3$(AO)(H$_2$O)$_2$$^+$ complex. Thus, due to the consistency between experimental and computational data indicating that hydrated formamidoximate-dioxovanadum(V) complexes are more stable than their corresponding hydrolyzed complexes, in what follows we will only investigate the interactions of formate and formamidoximate ligands with the hydrated VO$_2$$^+$ cation. However, since the relative population of the two forms can strongly depend on solution pH, ligand binding strength, and the presence of other ions, further investigation of the hydrolyzed species warrants a separate study.

12

VO$_2$(AO)(H$_2$O)$_3^+$,
0.00 (0.00)

H$_2$VO$_3$(AO)(H$_2$O)$_2^+$,
4.43 (2.03)
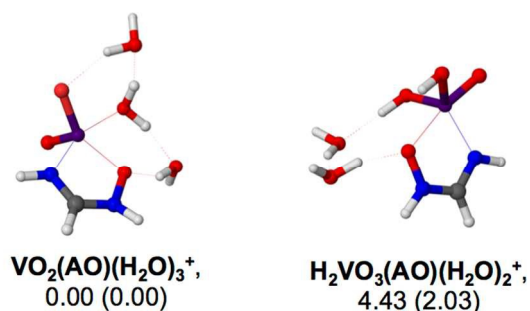
Figure 4. Structures of hydrated and hydrolyzed VO$_2$(AO)(H$_2$O)$_3$ complexes and relative energies in the gas phase and in aqueous solution (in parentheses) in units of kcal/mol.

3.3 Hydrated VO$_2^+$ Complexes

To gain insight into the discrepancy between experimental and previously computed coordination number of hydrated VO$_2$(H$_2$O)$_4^+$ complexes, relative energies of five- and six-coordinate species are computed. Prior reported DFT calculations (B3LYP/6-311+G(d,p) coupled with the SMD solvation model) predicted the VO$_2$(H$_2$O)$_4^+$ complex to be a five-coordinate structure,[16] while Car–Parrinello molecular dynamics (MD) simulations found the hydrated VO$_2^+$ complex to be an equilibrium mixture of five- and six-coordinate structures.[17] However, our results obtained at the CCSD(T) + δMP2 and MP2 levels are found to be in agreement with experimental EXAFS data, indicating that the six-coordinate VO$_2$(H$_2$O)$_4^+$ complex is more stable than the five-coordinate VO$_2$(H$_2$O)$_4^+$ conformer. The MP2 optimized VO$_2$(H$_2$O)$_4^+$ complexes and their relative CCSD(T) + δMP2 Gibbs free energies in the gas phase and in aqueous solution are shown in **Figure 5**, while the relative electronic energies are tabulated by level of theory in **Table 2**.

1, 0.00 (0.00)   **2**, 5.20 (5.50)
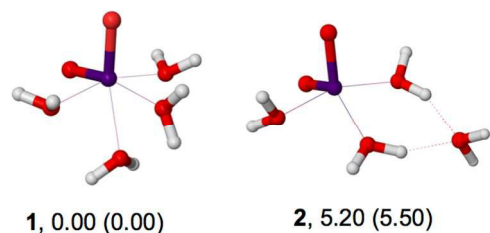
Figure 5. Structures of $VO_2(H_2O)_4^+$ complexes and relative energies in the gas phase and in aqueous solution (in parentheses) in units of kcal/mol.

Inspecting the results further, the five-coordinate $VO_2(H_2O)_4^+$ complex was favored by all density functionals except M06-L. Applying the D3 dispersion correction to B3LYP and M06-L did not significantly alter this result (<0.3 kcal/mol). However, these results are consistent with those obtained from the DFT optimization of the gas-phase VO_2^+ cation. This is due to the underestimation of the V=O bond length by DFT, which causes an increased stability in the anti-bonding character of the vanadium d-orbitals, consequently decreasing the coordination number of the VO_2^+ complexes. The M06-L density functional, which was parameterized for main-group and transition element thermochemistry, kinetics and noncovalent interactions[42] was an exception, likely due to the closer V=O bond lengths to the CCSD(T)/aug-cc-pVTZ results. We should note that clusters with only four water molecules might be too small to accurately predict the coordination number in bulk water. Nevertheless, the use of higher levels of theory provides greater consistency between the EXAFS and computational coordination number of the hydrated VO_2^+ ion.

Table 2. Relative gas phase electronic energies of five- and six-coordinate $VO_2(H_2O)_4^+$ clusters in kcal/mol.[a]

Theory	1 (c.n.= 6)	2 (c.n. = 5)
MP2	0.00	2.60
MP2/aug-cc-pVQZ//MP2	0.00	3.79
CCSD(T)//MP2	0.00	2.58
CCSD(T) + δMP2	0.00	3.77
B3LYP	3.88	0.00
CCSD(T)//B3LYP	0.00	0.90
M06	0.83	0.00
M06-L	0.00	0.89
ωB97XD	2.45	0.00
B97D3	2.86	0.00
PBE-D3	2.64	0.00
TPSS-D3	1.49	0.00
M06-L-D3	0.00	0.90
B3LYP-D3	2.21	0.00

[a]The aug-cc-pVDZ basis set was employed in all calculations unless otherwise specified. c.n. denotes coordination number.

3.4 Formate-VO_2^+ Complexes

Next, the relative energies of pure monodentate and bidentate carboxylate-VO_2^+ complexes are compared, in addition to investigating the preferred coordination number of simple $VO_2(HCOO)(H_2O)_x$ complexes (x = 1, 2). Based on CCSD(T)/aug-cc-pVDZ + δMP2 energies, the bidentate, five-coordinate $VO_2(HCOO)(H_2O)$ complex is slightly preferred over the monodentate, four-coordinate $VO_2(HCOO)(H_2O)$ complex (**Figure 6**). This result is consistent with the mixed carboxylate-amine, pyridine, and ether chelates observed for the majority of the carboxylate-VO_2^+ crystals in the CSD. However, this is in direct contrast to the formation of carboxylate-UO_2^{2+} complexes; UO_2^{2+} strongly prefers bidentate coordination of carboxylate ligands about its equatorial plane.[49]

3, 0.00 (0.00)   **4, 1.40 (1.56)**
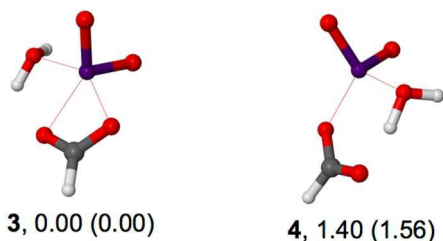
Figure 6. Structures of $VO_2(HCOO)(H_2O)$ complexes and relative energies in the gas phase and in aqueous solution (in parentheses) in units of kcal/mol.

The relative electronic energies of five- and four-coordinate $VO_2(HCOO)(H_2O)$ complexes are tabulated by level of theory in **Table 3**. With the exception of the B97D3 functional and the PBE functional with D3 corrections, the five-coordinate $VO_2(HCOO)(H_2O)$ complex was more stable than the four-coordinate one. Excluding the M06-L functional, all the DFT functionals underpredicted the stability of the five-coordinate $VO_2(HCOO)(H_2O)$ complex, which is again consistent with the underpredicted V=O bond lengths obtained from DFT. Conversely, MP2 overpredicted the stability of the five-coordinate $VO_2(HCOO)(H_2O)$ complex, which is consistent with the overpredicted V=O bond lengths obtained with MP2. Applying the

D3 correction to the B3LYP and M06-L density functionals did not significantly alter these

results (≤ 0.1 kcal/mol).

Table 3. Relative gas phase electronic energies of five- and six-coordinate $VO_2(HCOO)(H_2O)$ in kcal/mol.[a]

Theory	**3** (c.n. = 5)	**4** (c.n. = 4)
MP2	0.00	9.27
MP2/aug-cc-pVQZ//MP2	0.00	7.85
CCSD(T)//MP2	0.00	4.02
CCSD(T) + δMP2	0.00	2.60
B3LYP	0.00	0.05
CCSD(T)//B3LYP	0.00	5.61
M06	0.00	2.93
M06-L	0.00	4.49
ωB97XD	0.00	1.36
B97D3	1.33	0.00
PBE-D3	0.36	0.00
TPSS-D3	0.00	1.20
M06-L-D3	0.00	4.48
B3LYP-D3	0.00	0.05

[a]The aug-cc-pVDZ basis set was employed in all calculations unless otherwise specified. c.n. denotes coordination number.

Examining the effects of adding an additional water to form $VO_2(HCOO)(H_2O)_2$, it is observed that the five-coordinate complex, **5**, is far more stable than the six-coordinate complex, **8 (Figure 7)**. Furthermore, the monodentate five-coordinate $VO_2(HCOO)(H_2O)_2$ complex, **7**, is less stable than the bidentate five-coordinate carboxylate complex, **5**, by ~ 4 kcal/mol. This is likely due to hydrogen bond formed between the water and the unbound oxygen on the formate anion instead of the VO_2^+ oxygen. As a result, monodentate carboylate-VO_2^+ complexes should become more stable with additional water molecules, as they will provide additional stabilizing hydrogen bonds to both the carboxylate and the VO_2^+ cations. This hypothesis was confirmed with $VO_2(HCOO)(H_2O)_3$ complexes. The relative Gibbs free energies of these complexes in the gas phase and in aqueous solution can be found in **Figure S1** of the SI section. Applying the same reasoning, complex **6** is less stable than complex **5**, owing to the lack of hydrogen bonding with the VO_2^+ cation, while in complex **5**, the second water molecule is interacting with both the carboxylate oxygen and an oxygen atom on the VO_2^+ cation. Strong hydrogen-bonding ability of

oxygen atoms in VO_2^+ is consistent with the non-bonding character of one of their lone pairs (**Figure 2**).

5, 0.00 (0.00)   **6**, 3.06 (3.39)   **7**, 3.73 (3.97)

8, 9.89 (7.54)
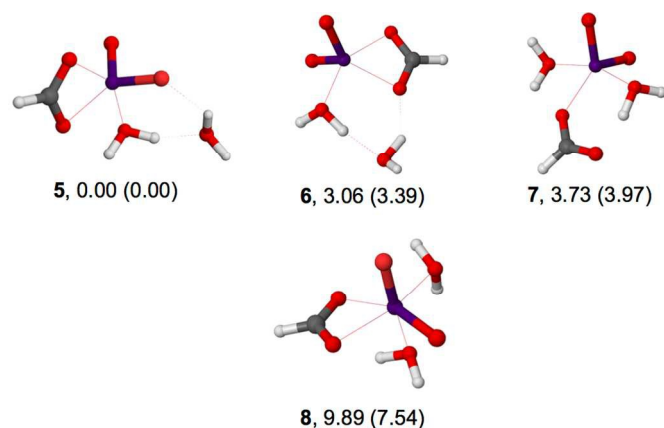
Figure 7. Structures of $VO_2(HCOO)(H_2O)_2$ complexes and relative energies in the gas phase and in aqueous solution (in parentheses) in units of kcal/mol.

Looking closer at the relative electronic energies of the five- and six-coordinate $VO_2(HCOO)(H_2O)_2$ complexes (**Table 4**), the seven density functionals employed in this study can be separated into two groups, functionals that behave like the B3LYP (ωB97XD, B97D3, PBE-D3, TPSS-D3, and B3LYP-D3) and functionals that behave like the M06 functional (M06L, M06-L-D3). Based on this grouping, DFT calculations of $VO_2(HCOO)(H_2O)_2$ were only carried out at the B3LYP and M06 levels of theory. Consistent with previous results, MP2 calculations overpredict the stability of the six-coordinate $VO_2(HCOO)(H_2O)_2$ complex, **8**, relative to the CCSD(T) prediction. Optimization of complex **8** at the CCSD/aug-cc-pVDZ level of theory resulted in a five-coordinated geometry, indicating that the six-coordinate structure is not a stationary point at this level. This result confirms that MP2 indeed significantly overestimated the stability of complex **8**. Likewise, the six-coordinate $VO_2(HCOO)(H_2O)_2$ complex is not stable at the B3LYP or M06 level of theory. The four-coordinate $VO_2(HCOO)(H_2O)_2$ complex was only located at the DFT level of theory. Single-point CCSD(T) calculations of the four-coordinate complex indicate that the stability of the complex is over-

predicted at the DFT level of theory. Along these lines, DFT calculations slightly under-predicted the stability of all three five-coordinate $VO_2(HCOO)(H_2O)_2$ complexes. In contrast, MP2 calculations incorrectly predicted complex **5** to be less stable than complexes **6** and **7**. It appears that MP2 calculations overpredict the stability of hydrogen bonds between the oxygen atoms on carboxylate anions and water molecules.

Table 4. Relative gas phase electronic energies of $VO_2(HCOO)(H_2O)_2$ complexes in kcal/mol.[a] All energies are given relative to the five-coordinate complex **5** in Figure 7.

Theory	**6** (c.n. = 5)	**7** (c.n. = 5)	**8** (c.n. = 6)	(c.n. = 4)[b]
MP2	-1.66	-1.84	0.69	
MP2/aug-cc-pVQZ//MP2	-1.73	-1.22	0.83	
CCSD(T)//MP2	1.55	0.76	7.71	
CCSD(T) + δMP2	1.48	1.38	7.85	
B3LYP	1.24	0.65		1.23
CCSD(T)//B3LYP	1.07	-0.51		6.70
M06	1.59	0.67		3.64

[a]The aug-cc-pVDZ basis was employed in all calculations unless otherwise specified. c.n. denotes coordination number.
[b]This structure is not illustrated in Figure 7, because it is not a stable minimum at the MP2 level of theory.

As eluded to in the discussion of $VO_2(HCOO)(H_2O)_2$, hydration effects will become greater with added waters. Accordingly, computations on $VO_2(HCOO)(H_2O)_3$ complexes were carried out at the same levels of theory as the $VO_2(HCOO)(H_2O)_2$ complexes (**Figure S1** and **Table S1**). These calculations further confirmed the higher instability of the six-coordinate complex at all levels of theory. Moreover, it was found that the five-coordinate monodentate $VO_2(HCOO)(H_2O)_3$ complex was energetically very similar to the five-coordinate bidentate $VO_2(HCOO)(H_2O)_3$ complex in aqueous solution, revealing that the average coordination mode is likely an equilibrium mixture of the two forms.

3.5 Formamidoximate-VO_2^+ Complexes

Moving now to the amidoxime ligand systems, the relative electronic energies of $VO_2(AO)(H_2O)$, $VO_2(AO)(H_2O)_2$, and $VO_2(AO)(H_2O)_3$ complexes are examined. CCSD(T) +

δMP2 energies of four- and five-coordinate $VO_2(AO)(H_2O)_n$ complexes are used as benchmarks against the DFT and MP2 optimized structures.

Starting with $VO_2(AO)(H_2O)$, surprisingly, the lowest energy complex obtained at the $CCSD(T) + \delta$MP2 level of theory was a five-coordinate amine nitrogen and oxime oxygen chelate complex **9** (**Figure 8**). This geometry entails a tautomeric rearrangement of the formamidoximate ligand, which leads to a structure that is ~5 kcal/mol more stable than the non-tautomeric form, **13** in aqueous solution. This indicates that the proton transfer between the amine nitrogen and the oxime nitrogen is essential to the formation of monoamidoxime-VO_2^+ complexes. Interestingly, the η^2 coordinating complexes **11** and **12** are found to be higher in energy (less stable) than the tautomeric species. This is an important result due to the fact that amidoxime-UO_2^{2+} η^2 complexes are generally more stable.[50] This has significant implications for the design of UO_2^{2+} selective ligands, a topic discussed in greater detail in the next section.

Monodentate formamidoximate-VO_2^+ complexes were investigated as well. A stable monodentate nitrogen complex, **10**, was obtained at the MP2 level. However, the monodentate oxygen complex converges into to an η^2 complex **12**. Complex **10** is less stable than complex **9** by ~1.5 kcal/mol in aqueous solution. Moreover, it should be noted that the formation of **10** entails proton transfer from the water ligand to the formamidoximate ligand. The neutralization of the formamidoximate ligand appears to have a stabilizing effect on complex **10**. Additionally, the formation of four-membered chelate rings via bidentate amine nitrogen and oxime nitrogen atoms, **15** and **14**, is far less stable than the formation of coordination modes depicted in **9-13**. Therefore, these coordination modes are not included in subsequent analysis of formamidxoimate-VO_2^+ complexes.

The relative electronic energies of the four- and five-coordinate $VO_2(AO)(H_2O)$ complexes are tabulated by level of theory in **Table 5**. With the exception of complex **10**, all calculations for $VO_2(AO)(H_2O)$ complexes consistent relative energies. Complex **10** is slightly more stable than **9** at the B3LYP, B97D3, and B3LYP-D3 levels (by 0.4−1.3 kcal/mol), while it is significantly less stable than **9** at the MP2 level (by 9.2−9.3 kcal/mol). Again, some overestimation of the instability of low-coordinate VO_2^+ complexes by MP2 calculations is consistent with the shorter bond lengths obtained from MP2 optimizations of bare, gas-phase VO_2^+ cations. On the other hand, DFT, MP2, and CCSD(T) predicted relative electronic energies of complexes of **9**, **12**, **13,** and **14** within 3 kcal/mol of the CCSD(T) + δMP2 value.
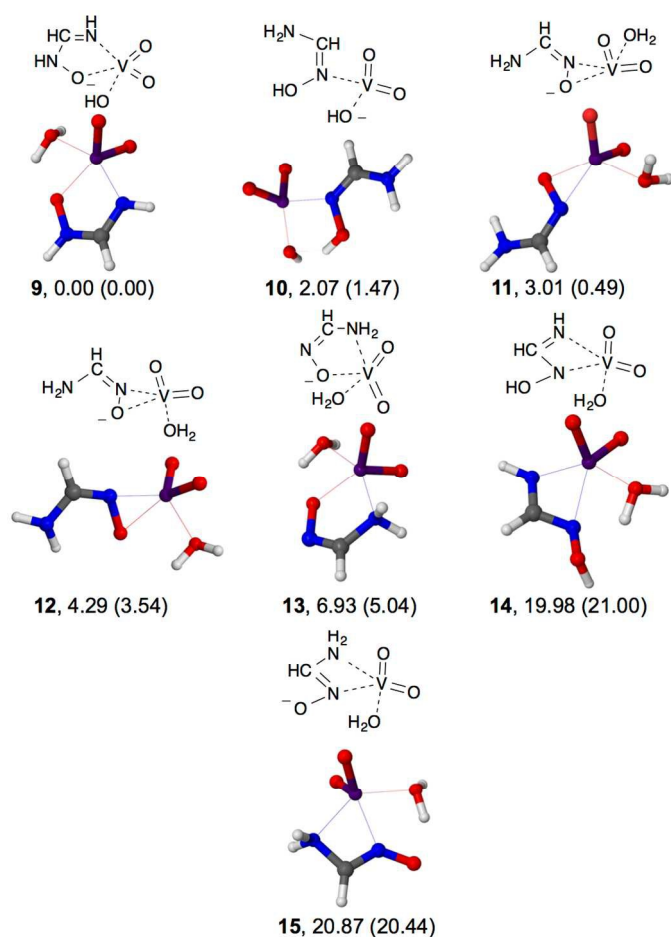
Figure 8. Structures of $VO_2(AO)(H_2O)$ complexes (AO=formamidoximate) and relative energies in the gas phase and in aqueous solution (in parentheses) in units of kcal/mol.

Table 5. Relative gas phase electronic energies of four- and five-coordinate VO$_2$(HAO)(H$_2$O) complexes in kcal/mol.[a] All energies are given relative to five-coordinate complex **9** in Figure 8.

Theory	10 (c.n.= 4)	11 (c.n.= 5)	12 (c.n.= 5)	13 (c.n.= 5)	14 (c.n.= 5)	15 (c.n.= 5)
MP2	9.19	9.91	6.49	6.64	18.14	16.91
MP2/aug-cc-pVDZ//MP2	9.31	9.74	6.52	8.98	19.50	18.67
CCSD(T)//MP2	3.47	5.30	5.96	5.01	19.86	19.39
CCSD(T) + δMP2	3.59	5.12	5.99	7.35	21.23	21.15
B3LYP	-0.52	4.89	4.60	9.34	22.71	19.65
M06	2.84	6.64	6.10	10.29	21.33	20.64
M06-L	3.69	4.76	4.81	9.19	21.73	18.88
ωB97XD	0.66	6.45	5.90	9.25	22.09	20.15
B97D3	-1.28	3.24	3.41	7.48	20.92	14.42
PBE-D3	0.53	3.93	4.10	8.71	21.42	14.49
TPSS-D3	1.05	4.07	4.42	7.85	21.10	15.27
M06-L-D3	3.67	4.76	4.81	9.20	21.74	18.88
B3LYP-D3	-0.38	5.56	5.18	8.73	22.04	18.98

[a]The aug-cc-pVDZ basis set was employed in all calculations unless otherwise specified. c.n. denotes coordination number.

Next, looking at systems containing two waters, VO$_2$(AO)(H$_2$O)$_2$ (**Figure 9**), results are consistent with those found in the monohydrate complexes. Specifically, the five-coordinate amine nitrogen and oxime oxygen tautomeric chelate, **16**, is the minimum energy structure Likewise, without the tautomeric rearrangement, structure **19** is predicted to be less stable. Again, similar to the monohydrate case, complex **18**, involving η^2 coordination, is only the third most stable complex. In addition, the complex formed from monodentate nitrogen coordination, complex **17**, is significantly more stable than the complex formed from monodentate oxygen coordination, **20**.

16, 0.00 (0.00)   **17**, 0.23 (1.62)   **18**, 2.24 (2.44)

19, 3.93 (3.18)   **20**, 9.04 (7.34)
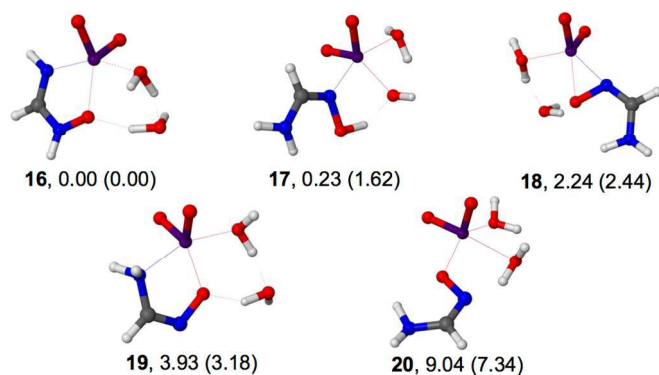
Figure 9. Structures of VO$_2$(AO)(H$_2$O)$_2$ complexes (AO=formamidoximate) and relative energies in the gas phase and in aqueous solution (in parentheses) in units of kcal/mol.

As mentioned in Section 3.3, the behavior of the DFT functionals employed in this study can be split into two groups, B3LYP-like and M06-like. Therefore, the B3LYP and M06 functionals were the only functionals tested for $VO_2(AO)(H_2O)_2$ and $VO_2(AO)(H_2O)_3$ complexes. MP2, CCSD(T), and DFT calculations consistently identified **16** as the most stable complex (**Table 6**). The relative stabilities obtained for complexes **16-20** at all levels of theory were within < 4 kcal/mol of the best method, except for **19**, where, as before B3LYP calculations overestimated the stability of the four-coordinate complex.

Table 6. Relative gas phase electronic energies of five-coordinate $VO_2(HAO)(H_2O)_2$ complexes in kcal/mol.[a] All energies are given relative to five-coordinate complex **16** in Figure 9.

Theory	17 (c.n. = 5)	18 (c.n. = 5)	19 (c.n. = 4)	20 (c.n. = 5)
MP2	3.68	4.37	11.71	5.22
MP2/aug-cc-pVQZ//MP2	4.04	4.17	11.95	6.60
CCSD(T)//MP2	1.72	4.22	9.91	3.62
CCSD(T) + δMP2	2.07	4.03	10.15	5.00
B3LYP	1.46	2.79	3.59	3.73
M06	1.51	1.57	7.10	7.49

[a]The aug-cc-pVDZ basis set was employed in all calculations unless otherwise specified. c.n. denotes coordination number.

Finally, analyzing three water systems, the tautomerically rearranged formamidoximate ligand complex is again found to be the most stable in the structures searched (**Figure 10**, complex **21**). Consistent with the results of the mono- and dihydrate complexes, structure **21** is ~4 kcal/mol more stable than the alternative tautomeric form **24.** The monodentate nitrogen **22** and the five-coordinate η^2 **23** are the second and third most stable complexes, respectively. We were also able to locate the six-coordinate η^2 complex, **25**, as a local minimum, but it was highly unstable.
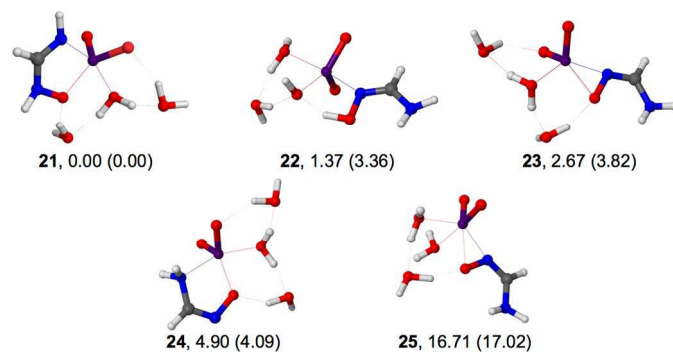
Figure 10. Structures of $VO_2(AO)(H_2O)_3$ complexes (AO=formamidoximate) and relative energies in the gas phase and in aqueous solution (in parentheses) in units of kcal/mol.

Compiling the relative electronic energies of the four- and five-coordinate trihydrate complexes (**Table 7**), it is again observed that CCSD(T), MP2 with large basis sets, and DFT calculations consistently identified **21** as the most stable complex. In regards to the six-coordinate complex, **25**, a stationary point on the MP2 potential energy surface was found, however not on the DFT potential energy surface. Given the significant instability of the complex, this structure was likely identified as a local minimum by MP2 calculations due to the tendency of MP2 to under-predict the stability of high coordination VO_2^+ complexes.

Table 7. Relative gas phase electronic energies of five- and six-coordinate $VO_2(HAO)(H_2O)_3$ complexes in kcal/mol.[a] All energies are given relative to five-coordinate complex **21** in Figure 10.

Theory	**22** (c.n. = 5)	**23** (c.n. = 5)	**24** (c.n. = 5)	**25** (c.n. = 6)
MP2	-0.38	3.76	5.69	9.00
MP2/aug-qz//MP2	0.64	3.81	7.34	10.04
CCSD(T)//MP2	0.25	4.12	4.48	15.22
CCSD(T) + δMP2	1.27	4.16	6.14	16.26
B3LYP	1.39	2.57	7.19	
M06	0.98	3.56	8.13	

[a]The aug-cc-pVDZ basis set was employed in all calculations unless otherwise specified. c.n. denotes coordination number.

3.6 Implications for Ligand Design

As mentioned in Section 3.3, the most stable binding motif obtained for $VO_2(AO)(H_2O)_n$, complexes (**9**, **16**, **21**) was a five-coordinate amine nitrogen and oxime oxygen chelate involving a tautomeric shift of hydrogen from the amide to oxime nitrogen atom. In modeling

complexation behavior of amidoximate ligands, an important question arises as to whether such tautomeric transformation is feasible in aqueous solution. The amidoxime-imino hydroxylamine tautomarization in the absence of complexing ions was investigated by Arshadi et al.[51] They reported that the energy barrier for tautomerization was prohibitively high in the gas phase (33-71 kcal/mol), but could be reduced substantially in the presence of explicit solvent molecules. Following this approach, we constructed a structural model for tautomerization of formamidoxime assisted by three water molecules, as seen in Figure 11. Consistent with the previous study,[51] the amidoxime form is ~9 kcal/mol more stable than the imino hydroxylamine form. The computed free energy barrier is ~25 kcal/mol for the forward and ~16 kcal/mol for the backward reaction. Since the relative stability of the two forms when bound to VO_2^+ is the opposite of that in the case of a free ligand, the reaction barrier involving the VO_2^+-amidoximate complex is expected to be $\leq$ 16 kcal/mol. Figure 12 provides an illustrative example of such complex, where, in addition to VO_2^+, five water molecules were placed into the system to adequately coordinate VO_2^+ and provide a pathway for proton transfer through a network of hydrogen bonds. We find that the transition state for the rate-limiting step lies only 9.5 kcal/mol above the initial complex, supporting very fast tautomeric proton exchange and equilibration to the most stable chelate structure.
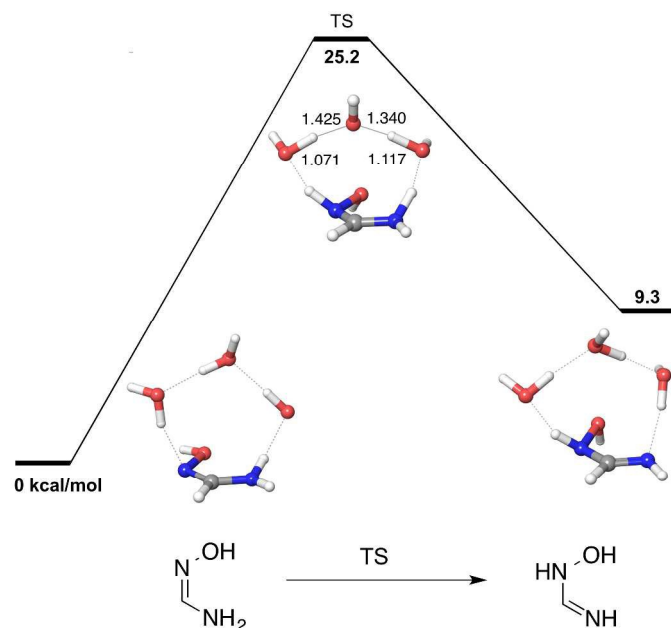
Figure 11. Reaction free-energy profile for tautomerization of formamidoxime calculated in the presence of three solvent (water) molecules (kcal/mol). Implicit solvation corrections are obtained using the IEF-PCM solvation model. DFT-optimized O−H bond lengths in the transition state are shown (Å).
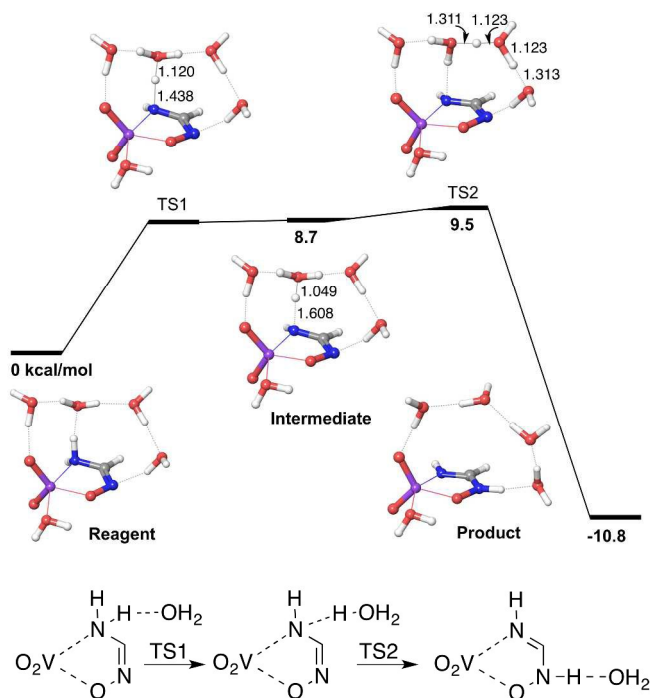
Figure 12. Reaction free-energy profile for tautomerization of formamidoximate coordinated to VO_2^+ in the presence of five solvent (water) molecules (kcal/mol). Implicit solvation corrections are obtained using the IEF-PCM solvation model. DFT-optimized O−H bond lengths in the transition and intermediate states are shown (Å).

While η^2 coordination of the oxime functional group is the most stable coordination mode of amidoximate-UO_2^{2+} complexes,[50] it is consistently found to be the third most stable coordination mode for those structures investigated. Based on these aforementioned results, it is suggested that the complexation between poly(acrylamidoxime) fibers and VO_2^+ cations can be restricted by either inhibiting the tautomeric rearrangement from the amidoxime to imino hydroxylamine via substitution of both amine hydrogens with alkyl groups or eliminating the amine group all together. Incorporating these concepts into ligands design will be an essential aspect to improving the UO_2^{2+} selectivity of future generations of chelating polymers.

Finally, searching the Cambridge Structural Database (CSD, 2014 release, version 5.36) for an unspecified transition metal and an amidoximate ligand with "any" bond specification for all carbon-nitrogen bonds and amine proton with no error and no disorder yielded 216 hits. These were further scrutinized to remove duplicate structures, structures containing amidoximate and imino hydroxylamine ligands that are not directly bonded to the metal center, structures that did not contain amidoximate or imino hydroxylamine ligands, and polynuclear complexes. As illustrated in **Figure 13**, the remaining 78 complexes can be classified into four categories: imino hydroxylamine-transition metal chelate complexes (**Type 1**) that are representative of the tautomerically rearranged formamidoximate-VO_2^+ binding motif observed in **9**, **16**, and **21**, monodentate oxime nitrogen complexes (**Type 2**) that are representative of the binding motif observed in **10**, **17**, and **22**, η^2 complexes (**Type 3**) that are representative of the binding motif observed in **11**, **18**, and **23**, and amidoximate-transition metal chelate complexes (**Type 4**) that are representative of the binding motif observed in **12**, **19**, and **24**. Approximately 78% of the complexes obtained were **Type 2** complexes, such as CIMMIW,[52] IMAXNI,[53] and YOHFEI.[54] Although the **Type 2** complexes were the most prevalent complexes, they were only observed

for bisamidoximate ligands and amidoximatee ligands linked to amines and pyridines. **Type 1** complexes, such as CUHJUK,[55] NEKLEW,[56] and POLFED,[57] are the most prevalent amidoximate complexes observed in the absence of additional amidoximates, amines, and pyridines (~ 18%). The remaining 4% of complexes observed were **Type 3**, such as RASBOC[58] and BASBIW.[58] However, RASBIW is listed as a **Type 4** complex in **Figure 12** because it was the only complex that exhibited the **Type 4** binding motif. These results lend merit to our observation, that in the absence of pyridines, amines, and additional amidoximate species, the most stable binding motif is the **Type 1** binding motif.
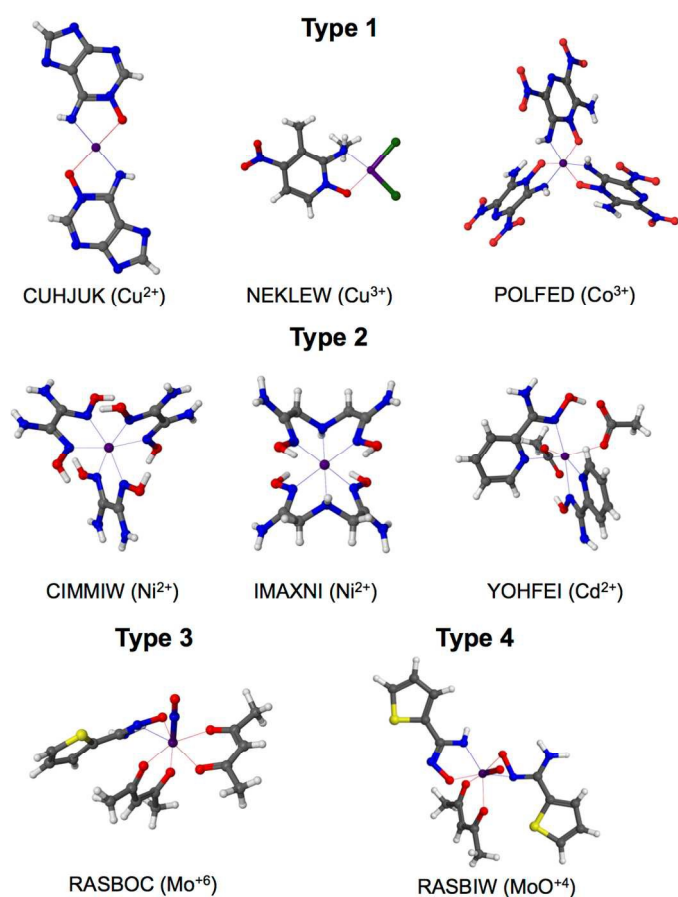
Figure 13. Crystal structures of amidoximate-transition metal complexes from the CSD. The **Type 1** complexes are representative of the tautomerically rearranged binding mode observed in complexes **9**, **16**, and **21**. The **Type 2** complexes are representative of the monodentate oxime nitrogen binding mode observed in complexes **10**, **17**, and **22**. The **Type 3** complex is representative of the η^2 binding mode observed in complexes **11**, **18**, and **23**. The **Type 4** complex is representative of the unrearranged binding motif observed in complexes **12**, **19**, and **24.**

Conclusion

In this work, we computationally elucidated the binding motif and coordination numbers of formamidoximate-VO_2^+ and formate-VO_2^+ complexes by investigating the relative energies of 25 formate-VO_2^+, formamidoximate-VO_2^+, and hydrated VO_2^+ complexes. We employed CCSD(T) calculations in the aug-cc-pVDZ basis set to determine benchmark relative energies of VO_2^+ complexes to evaluate MP2 and various DFT methods. Compared to the highest level of theory employed, DFT methods tend to underestimate, while MP2 tend to overestimate the coordination number of hydrated VO_2^+ complexes. In particular, CCSD(T) and MP2 calculations predict higher stability of the six-coordinate $VO_2(H_2O)_4^+$ complexes, compared to the five-coordinated complex where one of the water molecules is outside of the first shell, while all tested DFT methods yield the reversed stability of the two configurations. Thus, employing higher level of theory calculations has resolved the discrepancy between the experimental and computational coordination number of the hydrated VO_2^+ ion.

Moreover, our investigation of formate-VO_2^+ complexes revealed that the average coordination mode of pure carboxylate-VO_2^+ complexes in aqueous solution is an equilibrium mixture of monodentate and bidentate species. Our investigation of formamidoximate-VO_2^+ complexes universally identified the most stable binding motif formed by chelating a tautomerically rearranged imino hydroxylamine ligand via the amine nitrogen and the oxime oxygen. Transition state calculations identified the low-energy pathway for interconversion between the two forms, supporting fast rearrangement to the thermodynamically more stable tautomer. In contrast, previous studies showed the most stable amidoxime-UO_2^{2+} complexes are formed via η^2 coordination of the oxime functional group.[50] The difference in the binding motifs for complexation with UO_2^+ and VO_2^+ has important implications for ligand design. The UO_2^{2+}

selectivity of poly(acrylamidoxime) fibers could be improved by designing ligands that either contain only η^2 coordination sites of the oxime functional group or do not permit a tautomeric rearrangement from amidoxime to imino hydroxylamine by substituting both amine hydrogen atoms with alkyl group. The results provide an important step for developing a computational protocol for predicting the stability constants for VO_2^+ complexes. Combined with the demonstrated ability to predict the stability constants for UO_2^{2+} complexes,[59] this will provide the essential foundation for the rational design of ligands with enhanced uranyl affinity and selectivity.

Electronic supplementary information (ESI) available: Figure S1 showing structures of $VO_2(HCOO)(H_2O)_3$ complexes and relative energies in the gas phase and in aqueous solution, Table S1 listing relative electronic energies of $VO_2(HCOO)(H_2O)_3$ complexes at several levels of theory, and Cartesian coordinates of metal-ligand complexes accompanied with electronic energies of all species obtained with the B3LYP/aug-cc-pVDZ method and the MP2/aug-cc-pVDZ method, when available.

References

1.   J. S. Kim, C. Tsouris, R. T. Mayes, Y. Oyola, T. Saito, C. J. Janke, S. Dai, E. Schneider and D. Sachde, *Sep. Sci. Technol.*, 2013, **48**, 367-387.
2.   R. V. Davies, J. Kennedy, R. W. McIlroy, R. Spence and K. M. Hill, *Nature*, 1964, **203**, 1110−1115.
3.   K. Saito and T. Miyauchi, *J. Nucl. Sci. Technol.*, 1982, **19**, 145−150.
4.   G. R. Choppin, *Mar. Chem.*, 1989, **28**, 19-26.
5.   H. J. Schenk, L. Astheimer, E. G. Witte and K. Schwochau, *Sep. Sci. Technol.* , 1982, **17**, 1293-1308.
6.   L. Astheimer, H. J. Schenk, E. G. Witte and K. Schwochau, *Sep. Sci. Technol.*, 1983, **18**, 307−339.
7.   D. L. Wang and S. A. Sañudo Wilhelmy, *Mar. Chem.*, 2009, **117**, 52-58.
8.   T. Suzuki, K. Saito, T. Sugo, H. Ogura and K. Oguma, *Anal. Sci.* , 2000, **16**, 429-432.
9.   G. Abbasse, B. Ouddane and J. C. Fischer, *Anal. Bioanal. Chem.*, 2002, **374**, 873-878.
10.   S. P. Kelley, P. S. Barber, P. H. K. Mullins and R. D. Rogers, *Chem. Commun.*, 2014, **50**, 12504-12507.
11.   T. Kawai, K. Saito, K. Sugita, A. Katakai, N. Seko, T. Sugo, T. Kawakami and J. Kanno, *Ind. Eng. Res. Chem.* , 2000, **39**, 2910-2915.
12.   T. Kawai, K. Saito, K. Sugita, T. Kawakami, J. Kanno, A. Katakai, N. Seko and T. Sugo, *Radiat. Phys. Chem.*, 2000, **59**, 405-411.
13.   F. H. Allen, *Acta Cryst. B*, 2002, **58**, 380-386.
14.   G. Süss-Fink, S. Stanislas, G. B. Shul'pin, G. V. Nizova, H. Stoeckli-Evans, A. Neels, C. Bobillier and S. Claude, *J. Chem. Soc., Dalton Trans.*, 1999, 3169-3175.
15.   J. Krakowiak, D. Lundberg and I. Persson, *Inorg. Chem.*, 2012, **51**, 9598-9609.
16.   F. Sepehr and S. J. Paddison, *Chem. Phys. Lett.* , 2013, **585**, 53-58.
17.   M. Bühl and M. Parrinello, *Chem. Eur. J.*, 2001, **7**, 4487-4494.
18.   M. J. Frisch, G. W. Trucks, H. B. Schlegel, G. E. Scuseria, M. A. Robb, J. R. Cheeseman, G. Scalmani, V. Barone, B. Mennucci, G. A. Petersson, H. Nakatsuji, M. Caricato, X. Li, H. P. Hratchian, A. F. Izmaylov, J. Bloino, G. Zheng, J. L. Sonnenberg, M. Hada, M. Ehara, K. Toyota, R. Fukuda, J. Hasegawa, M. Ishida, T. Nakajima, Y. Honda, O. Kitao, H. Nakai, T. Vreven, J. A. Montgomery, Jr. , J. E. Peralta, F. Ogliaro, M. Bearpark, J. J. Heyd, E. Brothers, K. N. Kudin, V. N. Staroverov, R. Kobayashi, J. Normand, K. Raghavachari, A. Rendell, J. C. Burant, S. S. Iyengar, J. Tomasi, M. Cossi, N. Rega, M. J. Millam, M. Klene, J. E. Knox, J. B. Cross, V. Bakken, C. Adamo, J. Jaramillo, R. Gomperts, R. E. Stratmann, O. Yazyev, A. J. Austin, R. Cammi, C. Pomelli, J. W. Ochterski, R. L. Martin, K. Morokuma, V. G. Zakrzewski, G. A. Voth, P. Salvador, J. J. Dannenberg, S. Dapprich, A. D. Daniels, Ö. Farkas, J. B. Foresman, J. V. Ortiz, J. Cioslowski and D. J. Fox, *Journal*, 2009.
19.   M. Valiev, E. J. Bylaska, N. Govind, K. Kowalski, T. P. Straatsma, H. J. J. van Dam, D. Wang, J. Nieplocha, E. Apra, T. L. Windus and W. A. de Jong, *Comput. Phys. Commun.* , 2010, **181**, 1477-1489.
20.   G. D. Purvis and R. J. Bartlett, *J. Chem. Phys.*, 1982, **76**, 1910-1918.
21.   K. Raghavachari, G. W. Trucks, J. A. Pople and M. Head-Gordon, *Chem. Phys. Lett.*, 1989, **157**, 479-483.
22.   J. D. Watts, J. Gauss and R. J. Bartlett, *J. Chem. Phys.* , 1993, **98**, 8718−8733.

23.   T. H. J. Dunning, *J. Chem. Phys.*, 1989, **90**, 1007-1023.
24.   R. A. Kendall, T. H. J. Dunning and R. J. Harrison, *J. Chem. Phys.*, 1992, **96**, 6796-6806.
25.   M. Head-Gordon, J. A. Pople and M. J. Frisch, *Chem. Phys. Lett.*, 1988, **153**, 503-506.
26.   C. Møller and M. S. Plesset, *Phys. Rev.* , 1934, **46**, 618-622.
27.   P. Hohenberg and W. Kohn, *Phys. Rev.* , 1964, **136**, B864−B871.
28.   W. Kohn and L. J. Sham, *Phys. Rev.* , 1965, **140**, A1133−A1138.
29.   B. P. Hay and W. R. Wadt, *J. Chem. Phys.*, 1985, **82**, 270-283.
30.   B. P. Hay and W. R. Wadt, *J. Chem. Phys.*, 1985, **82**, 299-310.
31.   P. J. Hay and W. R. Wadt, *J. Chem. Phys.*, 1985, **82**, 284-298.
32.   L. E. Roy, P. J. Hay and R. L. Martin, *J. Chem. Theory Comput.* , 2008, **4**, 1029-1031.
33.   A. Ricca and C. W. Bauschlicher Jr., *Theor. Chim. Acta*, 1995, **92**, 123-131.
34.   J. P. Perdew, K. Burke and M. Ernzerhof, *Phys. Rev. Lett.*, 1996, **77**, 3865-3868.
35.   J. P. Perdew, K. Burke and M. Ernzerhof, *Phys. Rev. Lett.*, 1997, **78**, 1396.
36.   A. D. Becke, *J. Chem. Phys.* , 1993, **98**, 5648−5652.
37.   C. Lee, W. Yang and R. G. Parr, *Phys. Rev. B*, 1988, **37**, 785−789.
38.   J.-D. Chai and M. Head-Gordon, *J. Chem. Phys.*, 2008, **128**, 084106.
39.   J.-D. Chai and M. Head-Gordon, *Phys. Chem. Chem. Phys.*, 2008, **10**, 6615-6620.
40.   S. Grimme, *J. Comp. Chem.*, 2006, **27**, 1787-1799.
41.   S. Grimme, S. Ehrlich and L. Goerigk, *J. Comp. Chem.* , 2011, **32**, 1456-1465.
42.   Y. Zhao and D. G. Truhlar, *Theor. Chem. Acc.*, 2008, **120**, 215-241.
43.   J. M. Tao, J. P. Perdew, V. N. Staroverov and G. E. Scuseria, *Phys. Rev. Lett.*, 2003, **91**, 146401.
44.   S. Grimme, J. Antony, S. Ehrlich and H. Krieg, *J. Chem. Phys.*, 2010, **132**, 154104.
45.   E. Cancès and B. Mennucci, *J. Mater. Chem.*, 1998, **23**, 309−326.
46.   E. Cancès, B. Mennucci and J. Tomasi, *J. Chem. Phys.* , 1997, **107**, 3032−3041.
47.   B. Mennucci, E. Cancès and J. Tomasi, *J. Phys. Chem. B*, 1997, **101**, 10506−10517.
48.   S. Cotton, *Lanthanide and Actinide Chemistry*, Wiley, Hoboken, New Jersey, USA, 2006.
49.   J. Su, K. Zhang, W. H. E. Schwarz and J. Li, *Inorg. Chem.*, 2011, **50**, 2082-2093.
50.   S. Vukovic, L. A. Watson, S. O. Kang, R. Custelcean and B. P. Hay, *Inorg. Chem.* , 2012, **51**, 3855−3859.
51.   H. Tavakol and S. Arshadi, *J. Mol. Model*, 2009, **15**, 807−816.
52.   J. Nenwa, P. L. Djonwouo, M. M. Bélombé, E. N. Nfor and F. Emmerling, *ScienceJet* 2013, **2**, 43.
53.   D. L. Cullen and E. C. Lingafelter, *Inorg. Chem.*, 1970, **9**, 1865-1877.
54.   J. Liu, *Acta Crystallogr., Sect. E: Struct. Rep. Online*, 2014, **70**, 142-144
55.   E. Sletten, T. Marthinsen and J. Sletten, *Inorg. Chim. Acta*, 1984, **93**, 37-41.
56.   A. Puszko, A. Kochel, J. Wietrzyk, B. Filip-Psurska, J. Jezierska, M. Puszyńska-Tuszkanow, Z. Staszak, A. Adach, J. Lorenc and M. Cieslak-Golonka, *Polyhedron*, 2013, **50**, 146-153.
57.   J.-J. Liu, Z.-L. Liu and J. Cheng, *Chinese J. Inorg. Chem.*, 2014, **30**, 696-704.
58.   S.-G. Roh, A. Proust, F. Robert and P. Gouzerh, *J. Cluster Sci.*, 1996, **7**, 593-627.
59.   S. Vukovic, B. P. Hay and V. S. Bryantsev, *Inorg. Chem.*, 2015, **54**, 3995-4001.

Graphical Abstract

chelate, stronger binding

η², weaker binding

higher uranium selectivity